NASA/TM–2018-104606 / Vol. 51

Technical Report Series on Global Modeling and Data Assimilation, Volume 51

Randal D. Koster, Editor

The Atmosphere-Ocean Interface Layer of NASA's Goddard Earth Observing System Model and Data Assimilation System

Santha Akella and Max Suárez

National Aeronautics and
Space Administration

Goddard Space Flight Center
Greenbelt, Maryland 20771

July 2018

NASA STI Program ... in Profile

Since its founding, NASA has been dedicated to the advancement of aeronautics and space science. The NASA scientific and technical information (STI) program plays a key part in helping NASA maintain this important role.

The NASA STI program operates under the auspices of the Agency Chief Information Officer. It collects, organizes, provides for archiving, and disseminates NASA's STI. The NASA STI program provides access to the NASA Aeronautics and Space Database and its public interface, the NASA Technical Report Server, thus providing one of the largest collections of aeronautical and space science STI in the world. Results are published in both non-NASA channels and by NASA in the NASA STI Report Series, which includes the following report types:

- TECHNICAL PUBLICATION. Reports of completed research or a major significant phase of research that present the results of NASA Programs and include extensive data or theoretical analysis. Includes compilations of significant scientific and technical data and information deemed to be of continuing reference value. NASA counterpart of peer-reviewed formal professional papers but has less stringent limitations on manuscript length and extent of graphic presentations.
- TECHNICAL MEMORANDUM. Scientific and technical findings that are preliminary or of specialized interest, e.g., quick release reports, working papers, and bibliographies that contain minimal annotation. Does not contain extensive analysis.
- CONTRACTOR REPORT. Scientific and technical findings by NASA-sponsored contractors and grantees.
- CONFERENCE PUBLICATION. Collected papers from scientific and technical conferences, symposia, seminars, or other meetings sponsored or co-sponsored by NASA.
- SPECIAL PUBLICATION. Scientific, technical, or historical information from NASA programs, projects, and missions, often concerned with subjects having substantial public interest.
- TECHNICAL TRANSLATION. English-language translations of foreign scientific and technical material pertinent to NASA's mission.

Specialized services also include organizing and publishing research results, distributing specialized research announcements and feeds, providing help desk and personal search support, and enabling data exchange services. For more information about the NASA STI program, see the following:

- Access the NASA STI program home page at http://www.sti.nasa.gov
- E-mail your question via the Internet to help@sti.nasa.gov
- Phone the NASA STI Information Desk at 757-864-9658
- Write to:
  NASA STI Information Desk
  Mail Stop 148
  NASA's Langley Research Center
  Hampton, VA 23681-2199

NASA/TM–2018-104606/Vol. 51

Technical Report Series on Global Modeling and Data Assimilation, Volume 51

Randal D. Koster, Editor

The Atmosphere-Ocean Interface Layer of NASA's Goddard Earth Observing System Model and Data Assimilation System

Santha Akella
Science Systems and Applications, Inc., Lanham, MD
Max Suárez
Universities Space Research Association, GESTAR, Columbia, MD

National Aeronautics and
Space Administration

Goddard Space Flight Center
Greenbelt, Maryland 20771

July 2018

Level of Review: This material has been technically reviewed by technical management.

Available from

NASA STI Program
Mail Stop 148
NASA's Langley Research Center
Hampton, VA 23681-2199

National Technical Information Service
5285 Port Royal Road
Springfield, VA 22161
703-605-6000

Abstract

The Goddard Earth Observing System (GEOS) general circulation model (GCM) includes modules for sea surface temperature (SST) diurnal warming and cool-skin layers. To support the application of a coupled atmosphere-ocean data assimilation capability, the GCM needs to be flexible enough to support both coupled atmosphere ocean general circulation model (AOGCM) and atmosphere-only (AGCM) configurations, with only minor configuration changes at the user interface. This document presents a formulation of an atmosphere-ocean interface layer (AOIL) that serves this purpose. Previous work by Akella et al. (2017) described a version of a model for near-surface temperature variations, including both both diurnal warming and cool-skin effects, that has been used since 2017 in the near-real-time GEOS FP (forward processing) weather analysis and forecasting system. The diurnal cycle of SST in that version of the GEOS atmospheric data assimilation system (ADAS) undergoes a sharp decay in the late afternoon (local time). The updated AOIL presented here includes a modification of the similarity function used in the diurnal warming model. Results from offline model runs illustrate an improvement in the near-surface (less than 0.5m depth) diurnal cycle compared to the original formulation. The new formulation requires minimal parameter tuning, and the improvements are robust across long (several month) simulation periods. This new model formulation, however, retains some deficiences from the previous module, such as a small warm bias in calm wind conditions for water depths below 1m. Our future work would include surface salinification and sea-ice into the AOIL.

Contents

List of Tables

List of Figures

1 Introduction

The National Aeronautics and Space Administration (NASA) Goddard Earth Observing System (GEOS) model (Molod *et al.*, 2015, 2012) and data assimilation system (DAS) is used for a variety of applications: atmospheric data assimilation (Todling and El Akkraoui, 2018) and real-time forecasting (henceforth referred to as "Forward-Processing" (FP) System; https://gmao.gsfc.nasa.gov/GMAO_products/NRT_products.php), Modern-Era Retrospective Analysis For Research and Applications (MERRA), version 2 (Gelaro *et al.*, 2017) reanalysis, and seasonal forecasting (Borovikov *et al.*, 2017). The GEOS model used in the FP and reanalysis systems is an atmospheric general circulation model (AGCM), whereas the seasonal forecasting system relies on an atmosphere ocean general circulation model (AOGCM). Following the long-term goals laid out by the National Research Council (1992), National Academies of Sciences, Engineering, and Medicine (2018), NASA weather research objectives (Zeng *et al.*, 2016), and the World Weather Research Program (WWRP) recommendations, the Global Modeling and Assimilation Office (GMAO) is developing an atmosphere-ocean coupled data assimilation system (CDAS) (Brassington *et al.*, 2015; Dee *et al.*, 2014) which would use the GEOS AOGCM for all of the above applications.

Recently Akella *et al.* (2016, 2017) enhanced the sea surface temperature (SST) representation in the GEOS AGCM and atmospheric DAS by including a model for near-sea surface diurnal warming and cool-skin layers in order to resolve skin to bulk thermodynamic processes [1]. In contrast the GEOS AOGCM used for seasonal forecasting (Borovikov *et al.*, 2017) parameterizes the SST diurnal cycle (Ham *et al.*, 2014; Vernieres *et al.*, 2012) and does not include a cool-skin layer. The main objective of this paper is to document the formulation of a *unified* atmosphere-ocean interface layer (AOIL)[2] for the GEOS AGCM and AOGCM that paves the way for a future GEOS based CDAS; implementation details and results thereof are postponed to a future study. Another objective of this document is to describe an improvement to the diurnal warming model used in Akella *et al.* (2017) (henceforth referred to as ATS17). Gentemann and Akella (2018) and ATS17 showed that the diurnal warming of ATS17 decays unrealistically just after sunset; here we propose a modification to the ATS17 scheme to overcome this behaviour. Similarly formulated interface layers have already been implemented in the models of other operational centers, *e.g.*, in the European Center for Medium-Range Weather Forecasts (ECMWF) coupled model (Mogensen *et al.*, 2012), in the Norwegian Earth system model (Bentsen *et al.*, 2013), in the Geophysical Fluid Dynamics Laboratory (GFDL) coupled model (Delworth *et al.*, 2006), and in the UK Met Office HadGEM3 coupled model (Hewitt *et al.*, 2011). Akin to these examples, our interface layer also acts as a coupler between the atmosphere and ocean components. Besides this functionality, as in ATS17, the ultimate goal of the AOIL is to prognostically model the ocean surface variables (temperature, salinity, currents, waves, sea ice, etc) for improved assimilation of surface-sensitive observations, including satellite radiance observations. The formulation presented in this paper details a model for the near-surface ocean temperature variation only; future developments would extend our formulation to other surface variables of interest.

1.1 Document organization

This document is organized as follows. Section 2 describes the formulation of the AOIL for both AGCM and AOGCM implementations, focusing only on the modeling of near-surface temperature variations; a few recommendations are also provided for its potential near-future implementation in the GMAO seasonal forecasting system. Section 3 details the diurnal warming model used in ATS17

[1] operational since January 2017, GEOS version 5.16.5 onward

[2] pronounced "a-oil"; this acronym has no connection to any similar acronyms

and proposes a modified scheme that improves upon the ATS17 scheme. Section 4 provides results from off-line model simulations and observational comparisons. Section 5 provides a summary and conclusions.

2 Atmosphere-Ocean Interface Layer

The AOIL acts as a *coupler* of the atmosphere and ocean general circulation models (GCMs). Its chief objective is to provide the ocean general circulation model (OGCM) with surface fluxes from the atmospheric general circulation model (AGCM) while exchanging state variables among the two GCMs. We first describe the AOIL formulation in the general case of the coupled AOGCM; uncoupled AGCM case will be presented thereafter.

In order to accurately model the near-surface ocean temperature variations, we *embed* the model used by ATS17 into the top layer of the OGCM in such a manner that the OGCM needs no modification. See Alderson (1990), Schiller and Godfrey (2005), and Li *et al.* (2000) for similar formulations. The top layer of the OGCM, having depth D, is divided into two sub-layers, as shown in Fig. 1. The lower sublayer has a *foundation* temperature, T_f, which does not vary with depth within the sublayer. The subscripts, 'f' denotes the lower sublayer, 'w' denotes the upper sublayer and 'o' denotes the OGCM top layer. The upper or *interface* sublayer, i.e., the AOIL, has depth, d and contains the surface cool-skin layer and the diurnally varying warm layer; in this sublayer, temperature, $T(z)$ varies with depth.

We define T_w to be the mean temperature of the upper sublayer:

$$T_w = \frac{1}{d}\int_0^d T(z)\,dz, \tag{1}$$

and T_f to be the mean temperature of the lower sublayer:

$$T_f = \frac{1}{D-d}\int_D^d T(z)\,dz, \tag{2}$$

so that the mean temperature of the OGCM's top layer is given by

$$T_o = (1-\varepsilon_d)\,T_f + \varepsilon_d\,T_w, \tag{3}$$

where

$$\varepsilon_d = \frac{d}{D} < 1. \tag{4}$$

Typical values of d and D are 2 m and 10 m respectively[3]. We also define

$$\sigma_T = T_w - T_f, \tag{5}$$

which is the thermodynamic state variable of the AOIL or the top sublayer in Fig.1. The following relations, derived from above, will be useful:

$$T_w = T_o + (1-\varepsilon_d)\,\sigma_T, \qquad T_f = T_o - \varepsilon_d\,\sigma_T. \tag{6}$$

[3]If the OGCM has *sufficient* vertical resolution, $\varepsilon_d \sim O(1)$, and this formulation would have to be revised; a few recommendations are given in Appendix C

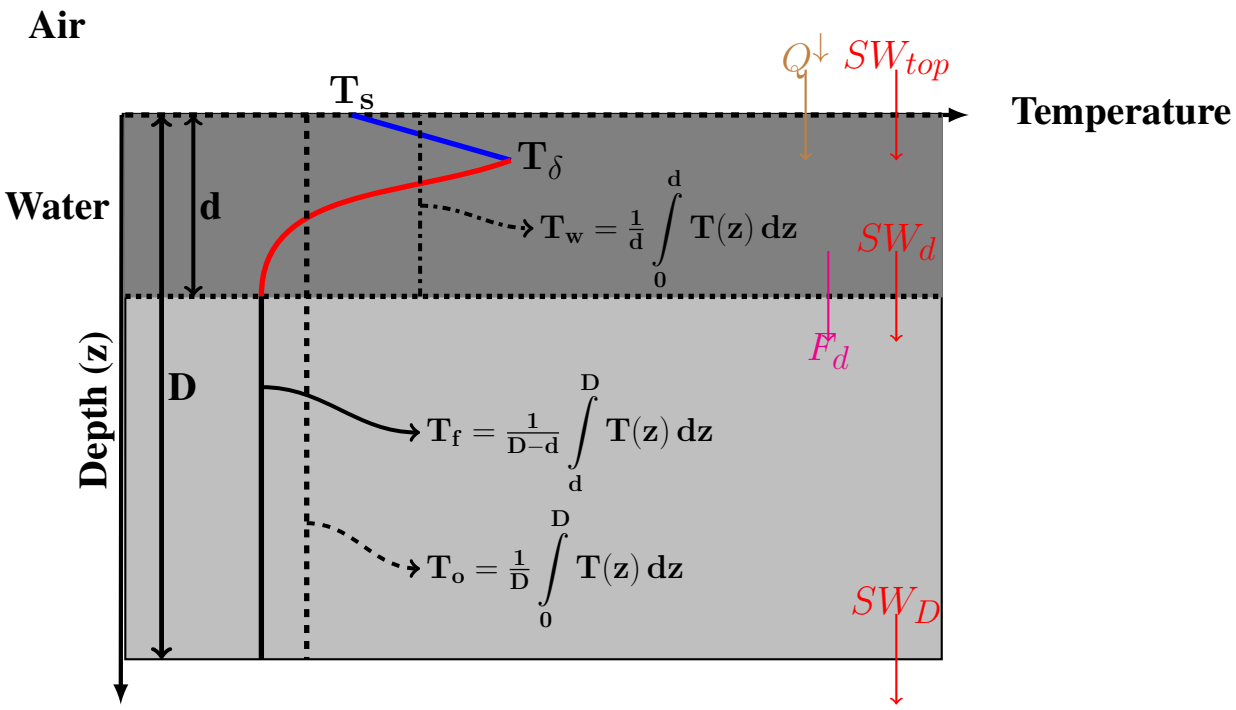

Figure 1: Schematic of the temperature variation in the top layer (depth: D) of the OGCM. The AOIL, or interface layer, (at depth, d, shown in dark gray) is above a foundation layer (shown in light gray). T_w, T_f and T_o are the depth-averaged temperatures in the interface, foundation and OGCM top layers, respectively. SW_{top} is the incident shortwave radiation at the top of the OGCM, and the radiation that penetrates through the interface and foundation layers is denoted by SW_d and SW_D respectively; the total contribution from the net longwave, latent and sensible heat fluxes at the top of the interface layer are denoted by $Q^{\downarrow}$ and F_d is the *local* turbulent flux at the base of the interface layer

.

In the interface and foundation layers, we assume that T_w and T_f evolve according to

$$d\,\rho_w\,c_w\,\frac{\partial T_w}{\partial t} = \underbrace{SW_{top} - SW_d + Q^{\downarrow}}_{=Q_w} + \varepsilon_d\,Q_O - F_d, \tag{7}$$

$$(D-d)\,\rho_w\,c_w\,\frac{\partial T_f}{\partial t} = \underbrace{SW_d - SW_D}_{=Q_f} + (1-\varepsilon_d)\,Q_O + F_d, \tag{8}$$

where $Q_w = SW_{top} - SW_d + Q^{\downarrow}$, $Q_f = SW_d - SW_D$, ρ_w and c_w denote the density and heat capacity of sea water and where F_d is the local turbulent heat flux at the base of the interface layer, which we assume is dominated by turbulent motions *within* the top layer of the OGCM (to be parameterized below). SW is the downward shortwave flux at the depth denoted by the subscript, and Q_O is the total contribution of heat from mixing, transport, and (in sea-ice covered regions) the freeze-melt potential computed by the OGCM. Q_O is assumed to be independent of depth within the topmost OGCM layer. The total heating from non-solar surface fluxes is given by

$$Q^{\downarrow} = LW^{\downarrow} - LW^{\uparrow}(T_s) - H_S(T_s) - H_L(T_s). \tag{9}$$

Here $LW^{\downarrow}$ is the downward longwave radiation absorbed by the surface, and the last three terms in (9), defined positive upward, are the emitted longwave radiation and the sensible and latent heat fluxes, respectively. These are assumed to depend on the surface skin temperature T_s, which will be diagnosed from the state variables as described below.

Multiplying Eq. (8) by $\frac{\varepsilon_d}{1-\varepsilon_d}$ and subtracting from Eq. (7) yields the following prognostic equation for σ_T:

$$d\,\rho_w\,c_w\frac{\partial\sigma_T}{\partial t} = \underbrace{Q_w - \frac{\varepsilon_d}{1-\varepsilon_d}Q_f}_{=Q_\sigma} - \frac{1}{1-\varepsilon_d}F_d. \tag{10}$$

Where

$$Q_\sigma = Q_w - \frac{\varepsilon_d}{1-\varepsilon_d}Q_f$$

Adding Eq. (7) and Eq. (8), and using Eq. (3), yields the OGCM's prognostic equation for T_o:

$$D\,\rho_w\,c_w\,\frac{\partial T_o}{\partial t} = Q_w + Q_f + Q_O. \tag{11}$$

In practice the atmosphere and ocean GCMs are coupled by an interface component that computes Q_w, Q_f, and F_d and updates σ_T. The OGCM updates T_o, computing Q_O and using the same Q_w and Q_f as the interface component. The main job of the interface component is to update its prognostic variable, σ_T, using (10). All other quantities in Fig. 1 must be prescribed or diagnosed from σ_T and the temperature of the top layer of the OGCM, T_o. Details of the algorithm, including the time discretization, will be given in following sections, but first we need a more detailed physical model of the warm and cool layers. For this we rely on the model proposed by Zeng and Beljaars (2005) (hereafter ZB05). They assume that the temperature within the interface layer varies as:

$$T(z) = \begin{cases} T_\delta - (1-\frac{z}{\delta})\Delta T_c & \text{if } 0 \le z \le \delta \rightarrow \textit{Cool Layer}, \\ \\ T_\delta - [\frac{z-\delta}{d-\delta}]^\mu (T_\delta - T_f) & \text{if } \delta < z \le d \rightarrow \textit{Warm Layer}, \end{cases} \tag{12}$$

where δ is the depth of the cool-skin layer (typically a few millimeters), T_δ is the temperature at $z=\delta$, μ is a scalar chosen to be ≤ 1, and $\Delta T_c = T_\delta - T_s$. Figures 2 and 3 depict an illustration of these variables and their typical diurnal variation, respectively. The temperature drop within the cool skin layer, ΔT_c, is calculated as in ATS17 (Appendix B).

Using Eq. (1), we can express T_w in terms of the above profile parameters in Eq. (12):

$$T_w = T_\delta - \frac{\delta}{2d}\Delta T_c - \frac{(1-\delta/d)}{(1+\mu)}(T_\delta - T_f),$$

Assuming $\frac{\delta}{d} \ll 1$,

$$T_\delta - T_w \approx \frac{1}{1+\mu}(T_\delta - T_f), \tag{13}$$

and

$$\sigma_T = T_w - T_f \approx \frac{\mu}{1+\mu}(T_\delta - T_f). \tag{14}$$

Using Eq. (6) and Eq. (14), we obtain the following relation

$$T_\delta \approx T_o + \left(\frac{1}{\mu} + (1-\varepsilon_d)\right)\sigma_T. \tag{15}$$

We also approximate the skin temperature as

$$T_s = T(z=0) \approx T_\delta - \Delta T_c. \tag{16}$$

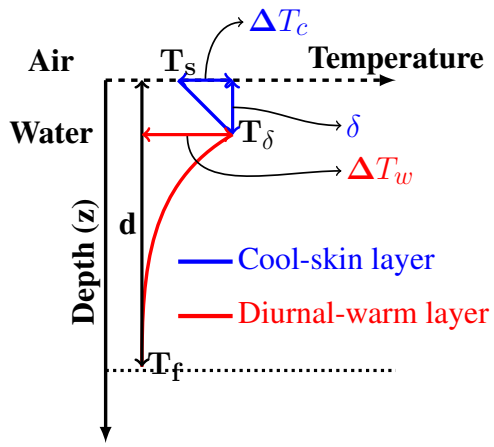

Figure 2: Details of the vertical variation of modeled temperature in the atmosphere-ocean interface layer of depth, d. T_f is the foundation temperature, T_δ is the temperature at the top of the diurnal warm layer, which has warmed by ΔT_w from T_f. The skin SST, T_s is cooler than T_δ by ΔT_c. Within the cool-skin layer (depth: δ) the temperature is assumed to vary linearly, whereas in the warm layer, it varies non-linearly; see text for details.

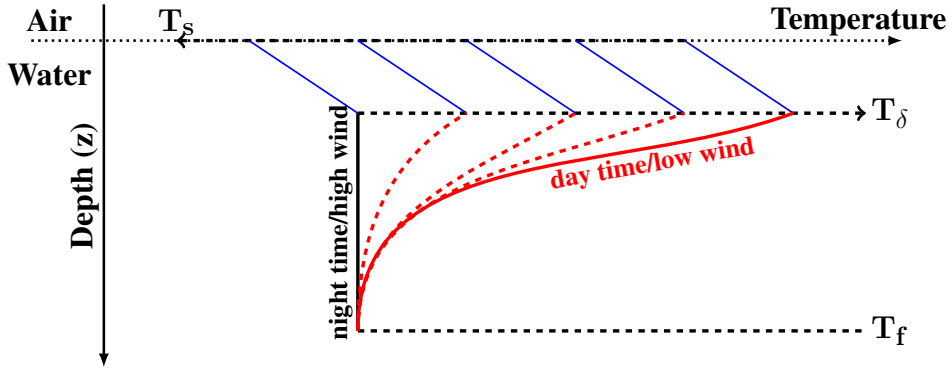

Figure 3: Schematic illustrating the modeled temperature profile in the AOIL. During local day time, in low wind conditions, positive ΔT_w shifts the profile to the right. Whereas at night time or high winds, $\Delta T_w \approx 0$, therefore $T_s \approx T_f - \Delta T_c$.

2.1 Turbulent heat flux at the base of the interface layer

Following ZB05 and ATS17, we assume that the turbulent heat flux at the base of the warm layer is given by

$$F_d = -\rho_w c_w \left[K(z) \frac{\partial T}{\partial z} \right]_{z=d}, \tag{17}$$

and using Eq. (12) and Eq. (14), we obtain

$$\left. \frac{\partial T}{\partial z} \right|_{z=d} = -\mu \left(\frac{T_\delta - T_f}{d - \delta} \right) \approx -(1+\mu) \frac{(T_w - T_f)}{d}, \tag{18}$$

so that Eq. (17) can be written in terms σ_T :

$$F_d = \rho_w c_w K(d)(1+\mu)\frac{\sigma_T}{d}, \tag{19}$$

From similarity theory, the diffusivity at depth d can be written as:

$$K(d) = \frac{\kappa u_* d}{\phi(\zeta)}, \tag{20}$$

where κ is the von Karman constant, $u_* = \sqrt{\frac{\tau_w}{\rho_w}}$ is the friction velocity in water, τ_w is the magnitude of the shear, and $\phi(\cdot)$ is an empirical similarity function operating on a non-dimensional measure of stability, ζ, with $\phi(0) = 1$ (details follow in section 3). Using equations (19) and (20), Eq. (10) can be rewritten as:

$$\frac{\partial \sigma_T}{\partial t} = \frac{Q_\sigma}{d\,\rho_w c_w} - \frac{1}{\tau_\sigma}\sigma_T, \tag{21}$$

where the turbulent relaxation time for σ_T is given by

$$\tau_\sigma = \frac{d^2(1-\varepsilon_d)}{K(d)(1+\mu)} = \frac{d(1-\varepsilon_d)\phi(\zeta)}{\kappa u_*(1+\mu)}. \tag{22}$$

To summarize the main computations, given Q_σ, we solve for the AOIL state variable σ_T using equation (21). T_δ and T_s are obtained by solving equations Eq. (15) and (16), respectively.

In the future, the GEOS DAS will be an atmosphere-ocean CDAS. The present operational version of the GEOS atmospheric DAS, though uncoupled to an ocean, uses the ATS17 based atmosphere-ocean interface layer for SST diurnal warm and cool-skin layers and will switch to the present formulation of AOIL to prepare for a future CDAS. Appendix C provides a few suggestions and remarks regarding the possible replacement of the parameterized SST diurnal cycle in the GMAO seasonal forecasting system with this formulation of the AOIL.

2.2 AGCM configuration

When the AOIL is exercised in the uncoupled, AGCM configuration, we simply ignore the Q_f term on the right-hand side of Eq. (10), i.e., $Q_\sigma = Q_w$. We also neglect ε_d when calculating the relaxation time-scale; therefore $\tau_\sigma = \frac{d\,\phi(\zeta)}{\kappa u_*(1+\mu)}$. Finally, T_f is read in from an already existing dataset; using (14) and (16) we calculate T_δ and T_s respectively. With the above simplifications we recover the formulation given by ATS17 and ZB05. Given the nature of these simple modifications, which keeps the core of the AOIL formulation intact between coupled and uncoupled GCM configurations, we have achieved our goal, outlined in section 1, of deriving a unified formulation.

3 Similarity function

Following Monin-Obukhov (M-O) similarity theory, ZB05 set $\zeta = z/L$, where

$$L = \frac{u_*^3}{\kappa F_B} \tag{23}$$

is the M-O length. The M-O length, which fully characterizes turbulence in the ocean's surface layer, depends only on the imposed surface quantities u_* and the buoyancy flux at the surface:

$$F_B = \frac{g\alpha}{\rho_w c_w} Q_w - \frac{c_w S\beta}{\alpha L_e} H_L(T_s), \tag{24}$$

where S is the near-surface salinity and α and β are the thermal and haline expansion coefficients of seawater, respectively, g denotes acceleration due to gravity, and L_e is the latent heat of vaporization. (Following ZB05, we ignore salinity effects on F_B.) This works well enough in the daytime when F_B is downward, and hence positive due to solar heating. Also, as long as u_* is *small*, F_d will be small, and the evolution of σ_T will be dominated by the surface heating. The problem with using M-O theory in the diurnal layer begins to appear at sunset (see discussion of similar to issues pointed by Schneider and Müller (1990) and Shinoda and Hendon (1998) for mixed layer models). The diffusivity very quickly becomes unrealistically large, since it is assumed to be in equilibrium with a negative buoyancy flux at the surface, when, in fact, the temperature profile is mostly stable and the turbulence is far from being in equilibrium with the surface flux. To remedy this problem, ZB05 use the net surface heating, Q_w in computing L only when L is positive, and when F_d defined in Eq. (19) is upward (i.e., negative) and $\sigma_T > 0$, they compute L by redefining the local buoyancy flux, F_B in Eq. (24) as follows:

$$F_B = \frac{g\alpha}{\rho_w c_w} F_d = \frac{g\alpha\kappa u_* (1+\mu)}{\phi}\,\sigma_T, \tag{25}$$

hence L and ζ will be always positive. ZB05 use the following stability function:

$$\phi(\zeta) = \begin{cases} 1+5\zeta & \zeta \geq 0, \\ (1-16\zeta)^{-1/2} & \zeta < 0. \end{cases} \tag{26}$$

Using the positive branch of above $\phi(\zeta)$ and the definition of L given in Eq. (23) and setting $\zeta = d/L$, we obtain

$$F_B = \frac{u_*^3(\phi-1)}{\kappa 5 d}. \tag{27}$$

Equating (25) and (27) gives the quadratic

$$\phi(\phi-1) = \kappa^2(1+\mu)\,\frac{5d\,g}{u_*^2}\,\alpha\sigma_T, \tag{28}$$

whose solution can be inserted in either (25) or (27) to obtain F_B. For $\phi \gg 1$, ZB05 arrived at following approximate solution (by setting $\phi \approx 5\zeta$ in Eq. (26))

$$\phi_s^2 \stackrel{\text{def}}{=} \kappa^2(1+\mu)\,\frac{f_\phi d\,g}{u_*^2}\,\alpha\sigma_T,\ f_\phi = 5, \tag{29}$$

instead of the following (positive) exact solution of Eq. (28),

$$\phi_e = \frac{1}{2}\left(1+\sqrt{1+g_\phi\,\phi_s^2}\right),\ g_\phi = 4. \tag{30}$$

Although results from ZB05 suggest that their treatment of turbulence may be adequate for a simple warm-layer model, it is still quite unsatisfying. After all, the fact that the turbulence is not in equilibrium with the surface buoyancy flux true not only after sunset, it's just obvious after sunset when $F_B < 0$. For small positive buoyancy flux, the turbulent mixing computed from (26) acts to destroy the warm layer too soon. Moreover, the turbulent heat flux F_d changes discontinuously, from a large neutral value when $F_B = 0$ to something much smaller immediately after the switch in their scheme (to calculate F_B). Guided by this reasoning, as mentioned in section 2.2 of ATS17, they opted to avoid having an abrupt change in σ_T, but at the expense of a rapid decay in σ_T; see ATS17 and Gentemann and Akella (2018) for further details. Note that other implementations of the ZB05 model also suffer from an abrupt decay in σ_T (see While and Martin (2013) and While

et al. (2017)). Large and Caron (2015) (see their figure 4) suggest another way (similar to ZB05) to introduce a *switch* in σ_T (to thereby avoid its its unrealistic drop). This approach is based on the overall ZB05 scheme, but uses a different formulation for the calculation of the diffusivity $K(d)$ in Eq. (20), that involves the computation of the Richardson number using a diurnally varying salinity and surface currents. We did not adopt the Large and Caron (2015) model due to this additional complexity and the undesirable switches, and our future plans of revising the AOIL (see section 1).

Figure 4 illustrates the solution of Eq. (21) for an idealized day, with constant values of u_*, and with insolation as in Large and Caron (2015). Here we set

$$SW_{top} = SW_{max} \sin^2 \left[2\pi \left(\frac{t - 6\,\text{hrs}}{24\,\text{hrs}} \right) \right],$$

between $t = 6 - 18\,\text{hrs}$, otherwise $SW_{top} = 0$. SW_{max} is set to 900 $\text{W}m^{-2}$, and the non-solar heat flux, $Q^{\downarrow}$, is set to -150 $\text{W}m^{-2}$. We used the Soloviev (1982) shortwave absorption profile $SW_z = \left[\sum_{i=1,3} a_i \exp(-z b_i)\right] SW_{top}$, to calculate SW_d and SW_D (see ZB05 for values of the coefficients $a_i, b_i, i = 1,3$); Q_σ and SW_{top} are shown in the inset. Other parameters were set to following values: $d = 2, D = 10, \mu = 0.2$.

Notice the behavior of σ_T in the late afternoon when the ZB05 scheme changes from surface M-O to local M-O, particularly in the calm wind ($u_* = 2\,mms^{-1}$) case; focus in particular on when the dash-dot (ATS17) and dashed (ZB05) lines deviate just after Q_σ changes sign. A plot of τ_σ clearly illustrates this problem with the ZB05 scheme; see Fig. 5.

Figure 4 also shows two limiting cases: the thin gray line shows the solution of Eq. (21) when turbulent mixing is ignored (i.e., neglecting the second term on the right hand side of (21)). The thick gray line is for neutral stability ($\phi = 1$, $u_* = 2\,mms^{-1}$) throughout the day. The former limiting case is essentially what ZB05, or any scheme, does in the warming phase for sufficiently light winds. In general, all solutions for schemes that are based on the general ZB05 model framework must lie between these two limits, and they will differ only in how they parameterize the stability dependence of F_d given in Eq. (17).

In order to obtain a continuous σ_T, while avoiding the unrealistic sharp decay as in ATS17, we simply use the ϕ_e given in Eq. (30) to calculate the relaxation time-scale τ_σ in Eq. (22); note that this stability function, ϕ_e, is independent of ζ. The solution of Eq. (21) with this simple change is shown in Fig. 4, and corresponding τ_σ is plotted in Fig. 5. Comparing ZB05 with our new scheme, we see that the latter has a slightly lower amplitude of σ_T for calm winds ($u_* = 2$ and $4\,mms^{-1}$), and is indistinguishable from ZB05 for larger u_*. Our new scheme avoids the sudden drop in σ_T and the discontinuity obtained with the ZB05 scheme. Since this is a simulation for an idealized day, we emphasize that one cannot judge from this comparison which solution is better. Results in section 4 include direct comparisons with observations.

4 Offline-line simulations with buoy observations

4.1 Data and simulation set-up

To validate our new scheme, we use buoy-measured temperatures and surface fluxes Woods Hole Oceanographic Institution (WHOI) Upper Ocean Processes Group (accessed in April, 2018). We consider data from three field campaigns: TOGA COARE (Weller and Anderson (1996), henceforth referred to as Coare), Arabian Sea Experiment (now onwards, Arabian Sea) and Spurs-1. Locations of these field campaigns are shown in Fig.6. We choose these specific data sets because they provide both temperatures and surface fluxes; see `http://uop.whoi.edu/projects/projects.`

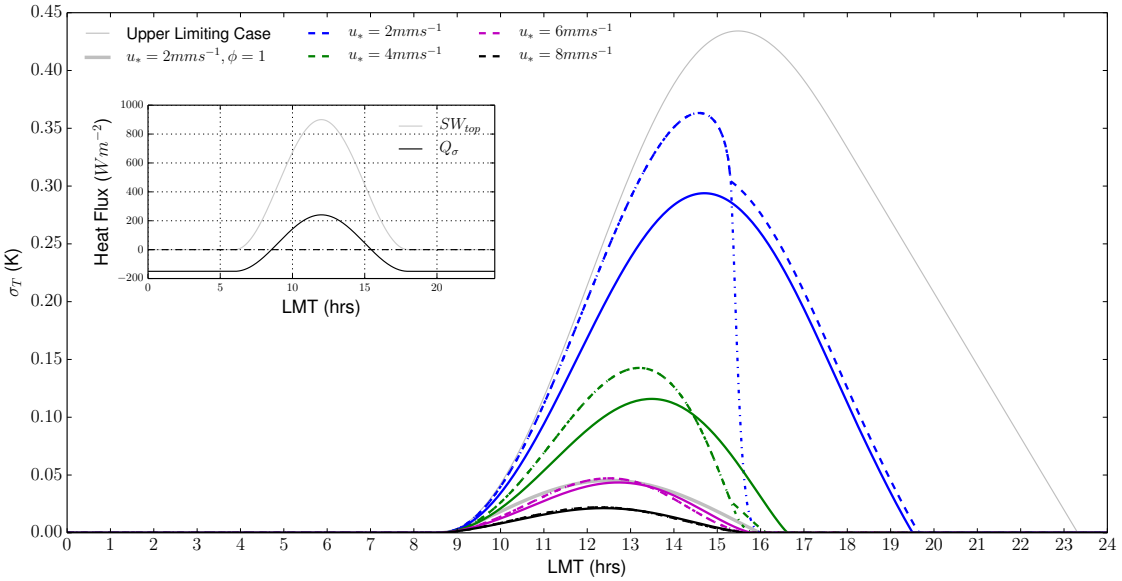

Figure 4: σ_T versus Local Mean Time (LMT) for an ideal day with constant u_* and $Q^{\downarrow} = -150$ Wm^{-2}. SW_{top} and Q_σ are shown in the inset. Two limiting cases are also shown in gray color: the upper limiting case (thin gray) ignores diffusive effects, and the lower limiting case (thick gray) is for $u_* = 2$ mm/s and neutral stability, $\phi = 1$. Dashed ('- -') lines are from the ZB05 model, dash dot ('-.') are from the ATS17 scheme which ignores stability effects in late afternoon, and solid ('–') lines are produced with the stability function given in Eq. (30). Blue, green, magenta and black color lines are for $u_* = 2, 4, 6$ and 8 mm/s, respectively. Note that results with the ATS17 and ZB05 schemes are identical until Q_σ changes sign in the late afternoon; thereafter there is a discontinuity in the evolution of σ_T with the ZB05 scheme, particularly for low values of u_*.

`html` for further details. In the following, our results are not restricted to short-term comparisons (one week to ten days as in ZB05 and Takaya *et al.* (2010)), but instead cover the entire duration of these field campaigns[4]. See Table 1 for start and end dates.

Table 1: Summary of data sets for offline simulations

Data Set	Location		Period (year/month/day)		Depth (m)	
	latitude (^{o}N)	longitude (^{o}E)	start date	end date	z_{top}	d
Coare	-1.76	155.99	1992/11/01	1993/03/01	0.45	2.00
Arabian Sea	15.50	61.50	1994/11/01	1995/10/01	0.17	1.91
Spurs-1	24.58	-38.00	2012/10/01	2013/09/01	1.30	2.10

Following the set-up of offline-simulations in ZB05 and Takaya *et al.* (2010), we compare our new scheme (henceforth referred to as NEW) with ZB05 and ATS17 in the AGCM configuration described in section 2.2. We opt for this configuration in order to compare with the ZB05 model, which was implemented in an AGCM. Therefore $Q_\sigma = Q_w$, with the depth of the AOIL, d, given in

[4]The first day of the month has been used only for the sake of convenience, without causing any change in the outcome of our simulations.

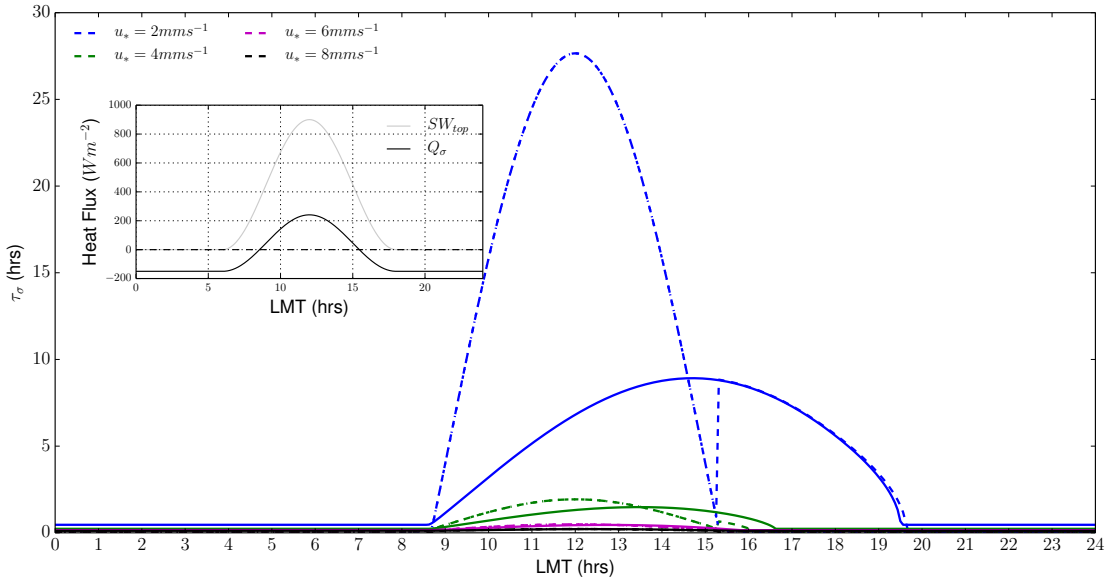

Figure 5: The relaxation time-scale, τ_σ in hours for the ZB05 scheme ('- -'), the ATS17 scheme ('-.'), and our new scheme ('–') for $u_* = 2, 4, 6$ and 8 mm/s (blue, green, magenta and black color lines, respectively). The inset plot is the same as in Figure 4. Note the discontinuity in τ_σ when the ZB05 scheme switches from surface to local M-O-based F_B.

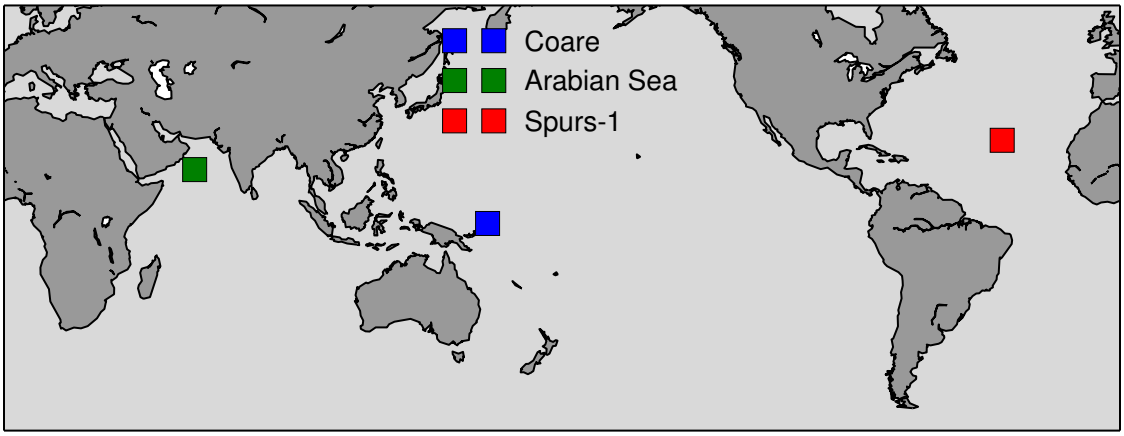

Figure 6: Locations and names of the data from field campaigns used for offline simulations

the last column of Table 1 for each of the above three data sets. Following ZB05 and as in section 3, for simplicity we use the Soloviev (1982) shortwave absorption profile to determine SW_d. The value of the exponent μ in the temperature profile Eq. (12) was set to 0.3; the sensitivity of the NEW scheme to μ will be discussed in section 4.2. Other variables ($SW_{top}, Q^{\downarrow}$ and u_*) are simply read from the WHOI data sets. Solution of Eq. (21) yields σ_T. Using the measured temperature at depth, d, as the foundation temperature, T_f, we can determine $T(z = z_{top})$ from equations (12) and (14); z_{top} is also given in Table 1.

Figures 7- 9 show time series of observed temperatures ($T(z = z_{top})$ and $T_f = T(z = d)$), Q_σ and u_* for the above three data sets. In calm winds and under high insolation, the temperature difference: $T(z_{top}) - T_d$ can exceed 3^oC, as in the Coare data around Dec 5, 1992 (Fig.7). The

Coare data set also exhibits consistently larger diurnal warming events than the other two, though this field campaign was for a shorter duration (Fig. 7- 9). Notice that during the night time or in high wind conditions, $T(z_{top}) - T_d$ approaches zero (as shown for the idealized day in Fig. 4) or can be negative due to nocturnal cooling or mixing (see, for example, Nov 10, 1992 and Jan 04, 1993 in Fig.7; Nov 01, 2012 in Fig.9). In the case of Spurs-1, the depths z_{top} and d are closer than in the other data sets, which could explain its smaller diurnal warming amplitudes seen in this case. Due to the ubiquitous nature of diurnal warming events in all three data sets, in the following subsections, we will compare the observed temperature difference $T(z_{top}) - T_d$ with the temperature differences produced by the ZB05, ATS17 and NEW schemes using averaged differences.

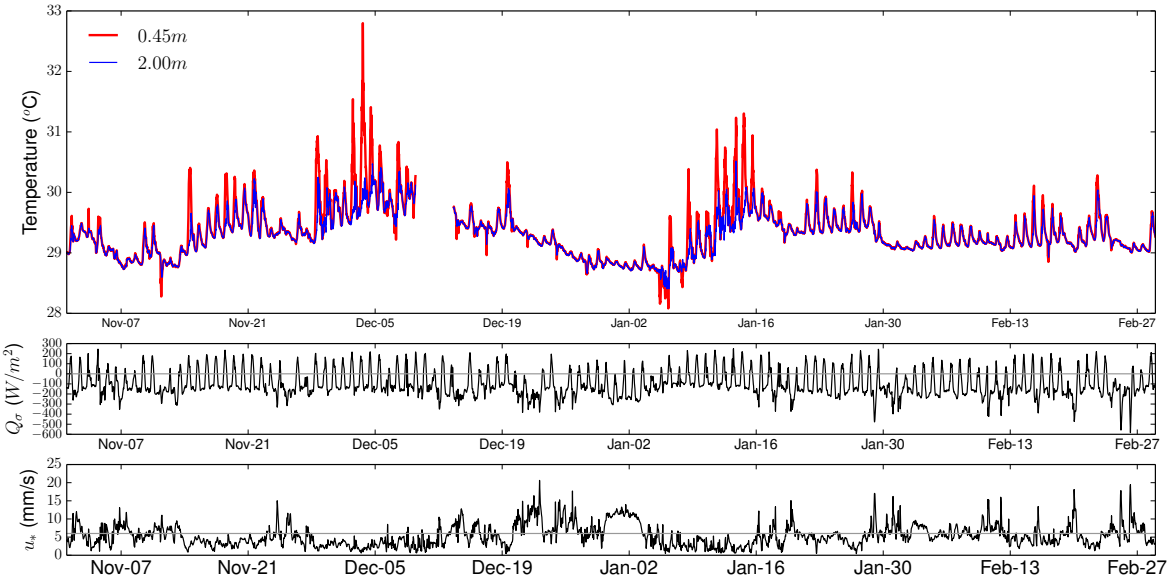

Figure 7: Time series of observed temperatures at z_{top} and d (top panel), heat flux (Q_σ, middle panel) and friction velocity in water (u_*, bottom panel) for the Coare data set.

4.2 Parameter tuning of the NEW scheme

Recall that the temperature profile, $T(z)$, in Eq. (12) and the relaxation time-scale, τ_σ in Eq. (22), both depend on the scalar μ. The other parameter that impacts τ_σ is f_ϕ in Eq. (29). As already stated in section 2, $\mu \in (0,1]$; for smaller values, $T(z)$ profile peaks closer to the surface (i.e., as $z \to 0$) and for larger values close to unity, we obtain a linear variation of the temperature profile with depth. Therefore it is obvious to expect that the temperature differences should be strongly affected by the choice of μ. On the other hand f_ϕ directly impacts the similarity function via Eq. (22), $\tau_\sigma \propto \phi$, and hence larger values of f_ϕ lead to longer relaxation time-scales. ZB05 set $\mu = 0.3$ and $f_\phi = 5$. In order to investigate the sensitivity of our NEW scheme to both μ and f_ϕ, we calculated the difference between our model predicted $T(z_{top})$ and corresponding observed values, for the entire duration of each of the data sets in Table 1 and over a range of values of these two parameters. The resulting *errors* were then binned into three wind speed *regimes*: low ($u_* \in [0,3)$ mm/s), medium ($u_* \in [3,6)$ mm/s) and high ($u_* \geq 6$ mm/s). Colormaps of the mean and standard deviation of these these differences for the three field campaigns are shown in Figures 10 and 11, respectively. For reference sake, values obtained with the ZB05 model using the above-noted parameter values are also shown (values for the ATS17 model are not shown because the results are similar to those for

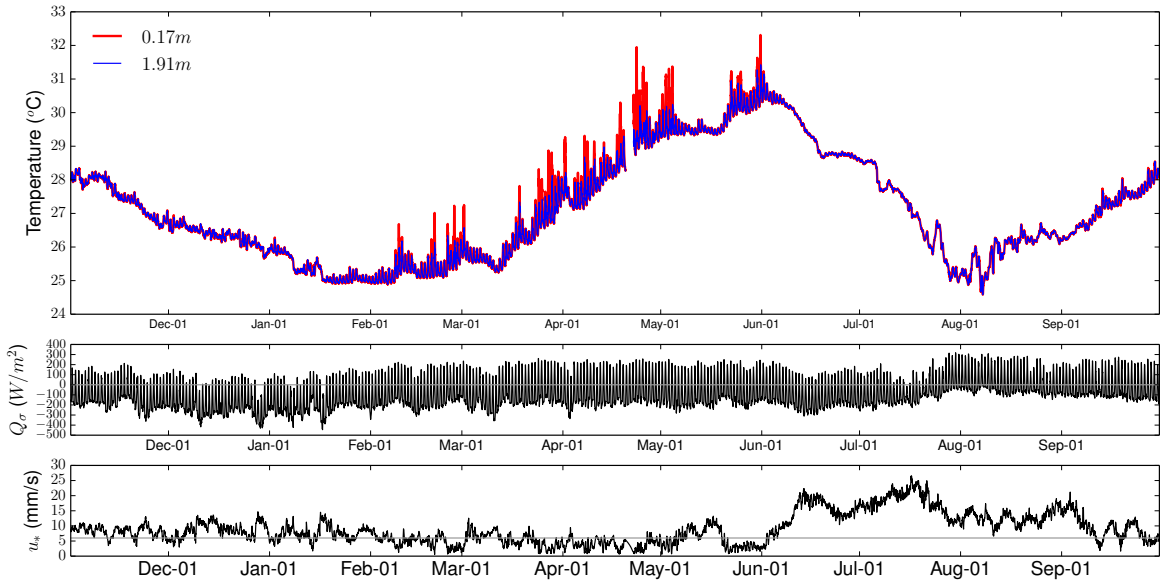

Figure 8: Same as Fig.7 but for the Arabian Sea Experiment.

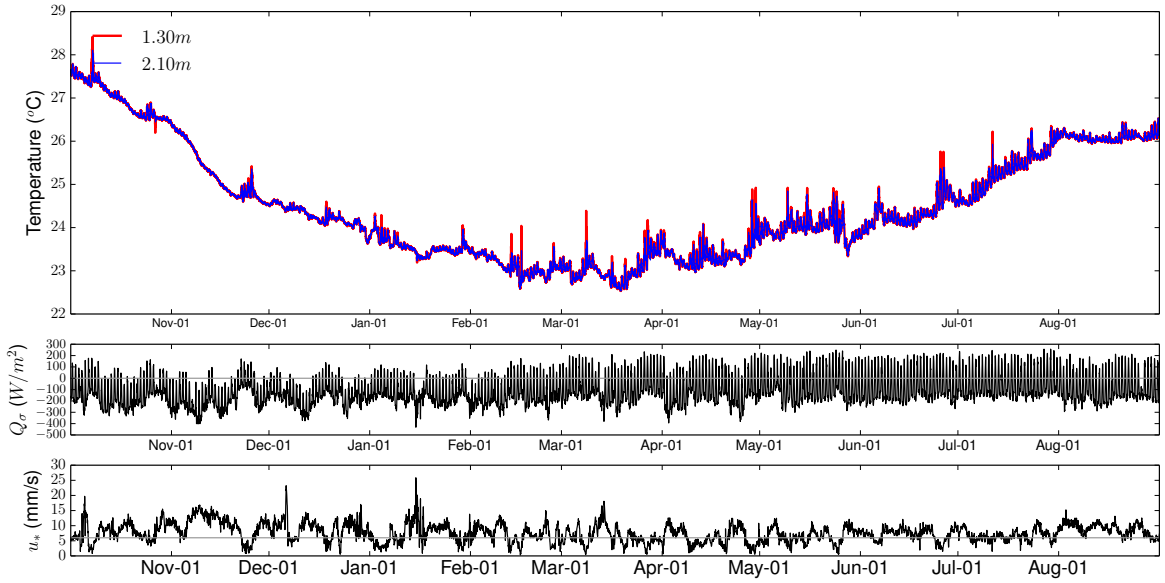

Figure 9: Same as Fig.7 but for the Spurs-1 field campaign.

the ZB05 model).

The largest errors (mean and standard deviation) were obtained for $\mu = 0.1$, and errors decreased with increasing μ, with a small negative mean error found for μ close to 1. Due to negligible stratification at high winds, the relatively small diurnal warming amplitude results in the smallest errors for $u_* \geq 6$mm/s. Based on the mean and standard deviations for all three cases, we chose $\{f_\phi, \mu\} = \{3, 0.3\}$. One can advocate for the application of a robust parameter estimation (Navon, 1998) procedure to determine the *optimal* set. However, we refrain from adopting such a procedure because, as shown in Figures 10 and 11, the error statistics vary based on the data set and wind speed regime. In other words, the error has a spatial variability, and it perhaps has a seasonal

variability because winds vary seasonally, though it is beyond the scope of this work to illustrate this. Ultimately the AOIL will be implemented in the GCM, and for such an implementation, the computational expense of online parameter estimation would not be negligible. For now we proceed with the above choice of the two parameters in our NEW scheme.

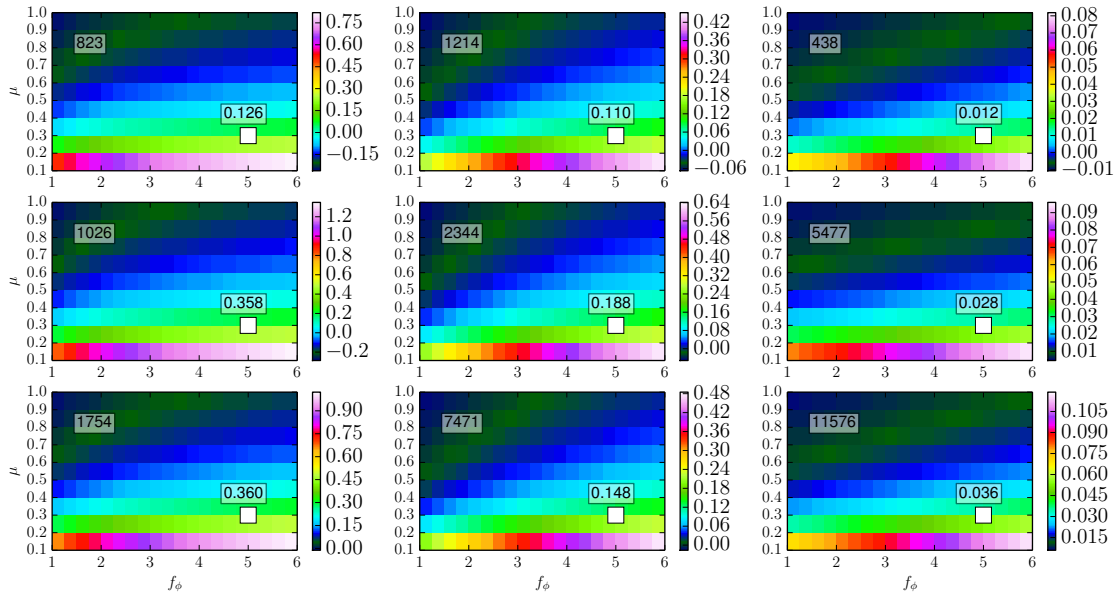

Figure 10: Time-averaged mean of the difference between observed and NEW scheme-predicted $T(z_{top})$ as a function of μ and f_ϕ. Top, middle and bottom rows are for the Coare, Arabian Sea and Spurs-1 datasets, respectively. Left, middle and right panels are for u_* contained within $[0,3)$, $[3,6)$ and $[6,\infty)$ mm/s, respectively. The number of samples for each case is shown in the top left corner. The ZB05 $\{f_\phi, \mu\}$ is marked with a white open square along with its mean value. Note the difference in colorscales.

4.3 Correlation between observed and modeled diurnal warming

We now compare the diurnal warming $T(z_{top}) - T_d$, from the observations against that from the ZB05, ATS17 and NEW schemes. As described in section 4.1, T_d is the observed temperature at depth d in all these cases. Figures 12- 14 show, for the three field campaign datasets, scatter plots of the observed and modeled diurnal warming for different wind speed regimes. Notice that our new scheme has the smallest standard deviation for the Coare and Arabian Sea datasets and has a standard deviation comparable to that of the other schemes for Spurs-1. We speculate that because of the deeper z_{top} for Spurs-1, all schemes have a significant departure from the best fit line. As noted earlier, the errors are significantly lower for high wind speeds. However, all the schemes are unable to capture the diurnal warming amplitude at these high wind speeds, and they consistently over predict the diurnal warming. Since the mean error is of the order of tenths of a centigrade, it is within the typical range of instrument uncertainties.

4.4 Diurnal variation as a function of wind speed

Now we compare the diurnal variability from our NEW scheme with that from the ATS17 scheme to show that our proposed formulation addresses the ATS17 scheme's issue of unrealistically rapid

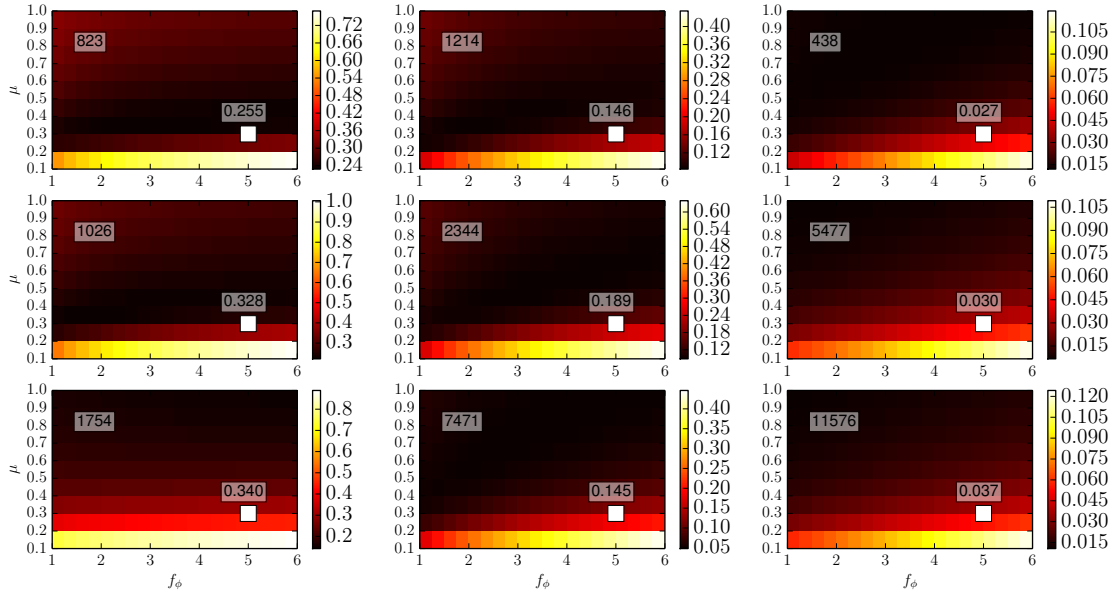

Figure 11: Same as Fig. 10 but for the standard deviation of the differences

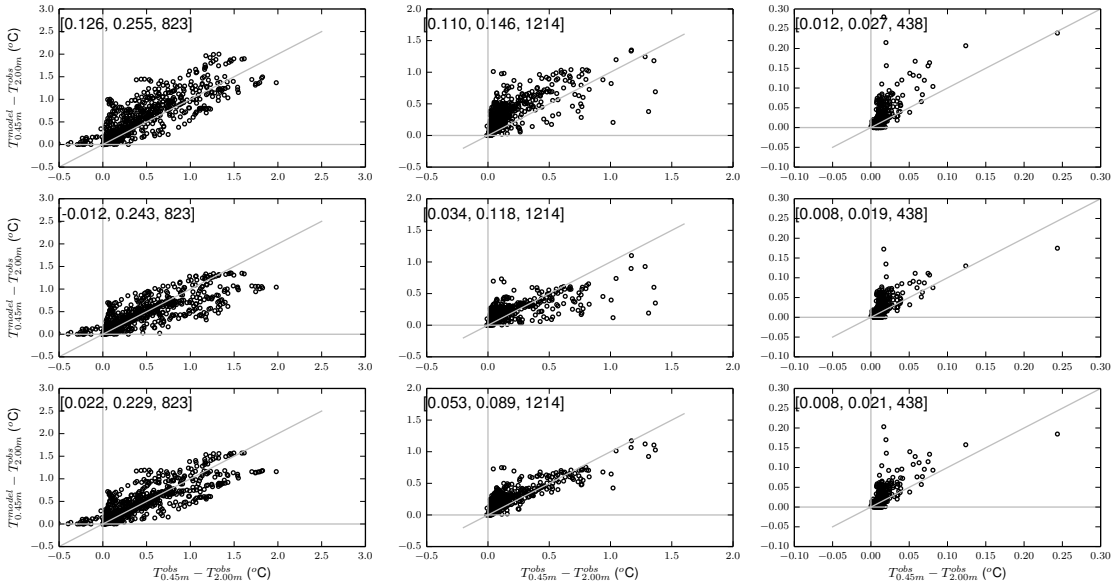

Figure 12: Scatter plot of the modeled and observed diurnal warming, calculated from temperature differences at $z = z_{top}$ and d, for the Coare field campaign. Top, middle and bottom rows are for the ZB05, ATS17 and NEW schemes respectively. As in Fig. 10, the left, middle and right panels are for u_* contained within the ranges $[0,3), [3,6)$ and $[6,\infty)$ mm/s, respectively. The mean, standard deviation, and number of data points are provided in the top left corner.

decay of diurnal warming (Gentemann and Akella, 2018). For reference, diurnal variability for the ZB05 scheme is also shown. Figures 15 - 17 show, for the three field campaigns, the averaged diurnal variability as a function of Local Mean Time (LMT) for low to high wind speed regimes. The problem with the ATS17 scheme is evident; the diurnal warming consistently decays by 4:30PM

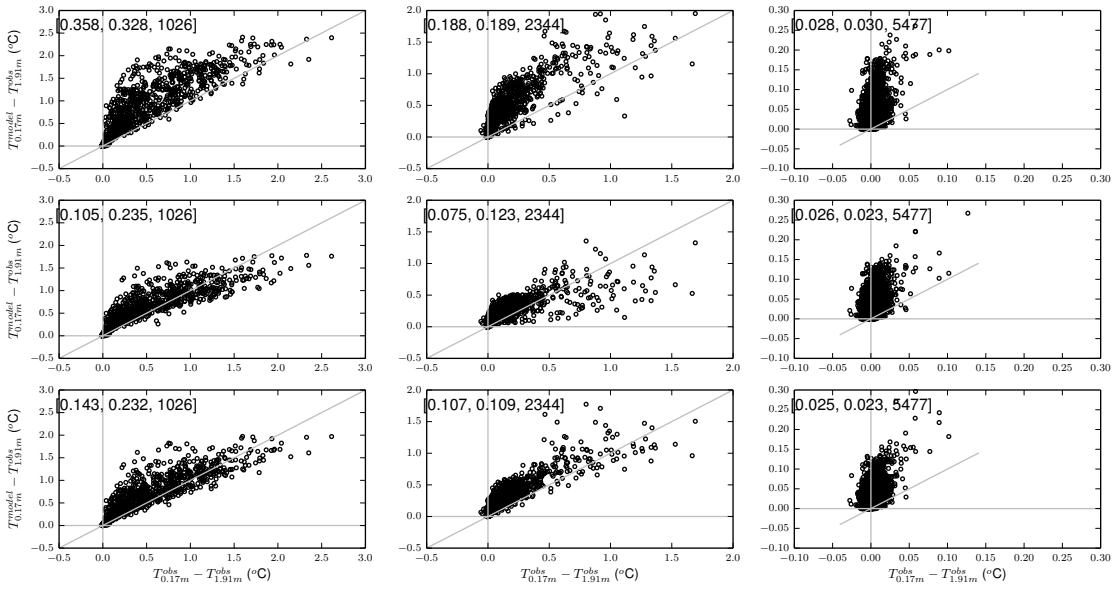

Figure 13: Same as Fig. 12, but for the Arabian Sea.

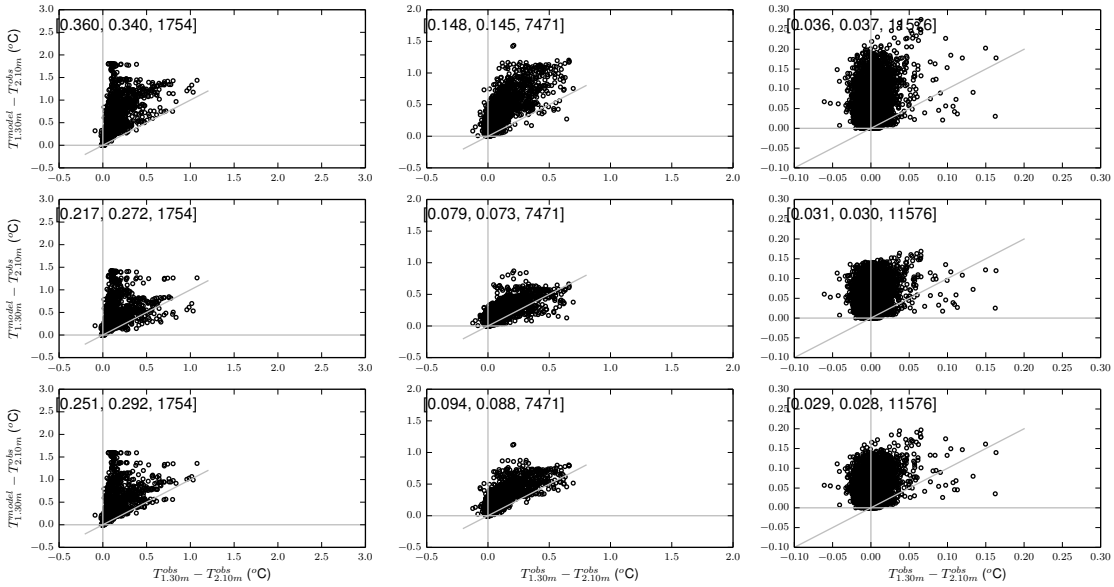

Figure 14: Same as Fig. 12, but for the Spurs-1.

LMT. Since the diurnal warming has been averaged over the duration of the field campaign, the discontinuous evolution of diurnal warming obtained with ZB05 (see section 3) cannot be seen. However, the ZB05 scheme over predicts the amplitude of diurnal warming for low wind speeds. For both the Coare and Arabian Sea datasets, both of these issues seem to be addressed by our NEW scheme (which uses, by the way, the parameter values described in section 4.2). Notice again that the Spurs-1 data set, with its deeper z_{top}, poses a difficulty for all of the schemes. For Spurs-1, the warm bias at low wind speeds is in excess 0.3^oC; we hope to address this issue in future work. Meanwhile, based on the results obtained with our NEW scheme, we feel encouraged to proceed with its implementation in the AOIL of the GEOS- GCM and DAS.

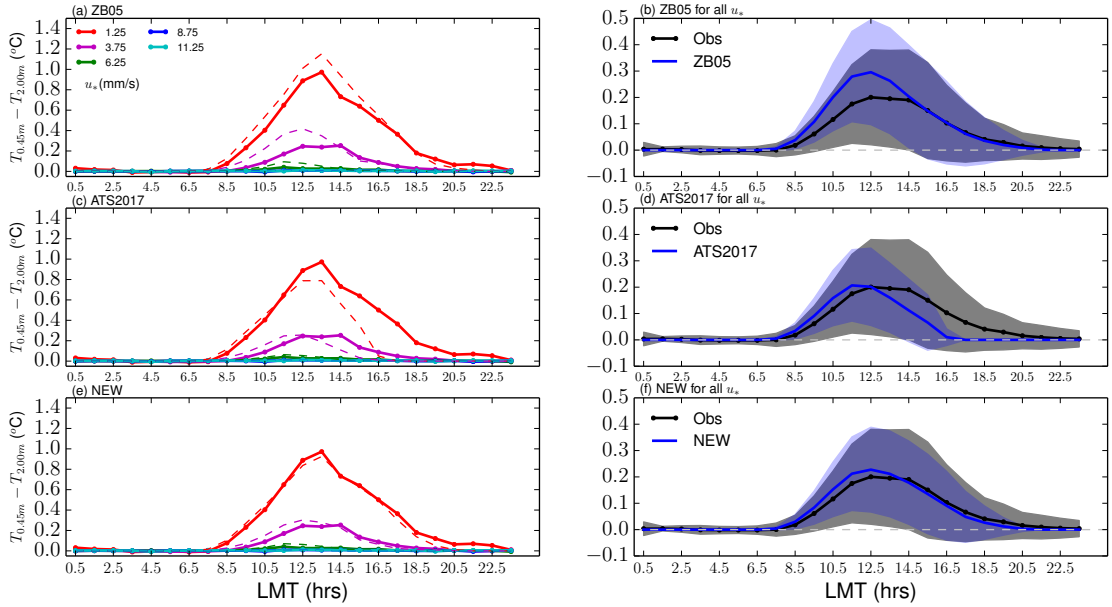

Figure 15: Comparison of Coare observed (solid lines) and modeled (dashed lines) averaged diurnal warming as a function of the Local Mean Time (LMT), for different wind speed regimes (left panels) and for all wind speeds (right panels). The top, middle and bottom panels are for the ZB05, ATS17 and NEW schemes, respectively. In the left panels, diurnal warming data were sorted into five bins of u_* values, each bin having a width of 2.5mm/s; the center of each bin is shown in the legend. The right panels also show $\pm$ half standard deviation of diurnal warming in shades of gray (observed) and blue (modeled). Due to averaging, notice the uneven evolution of diurnal warming in the (left) right panels.

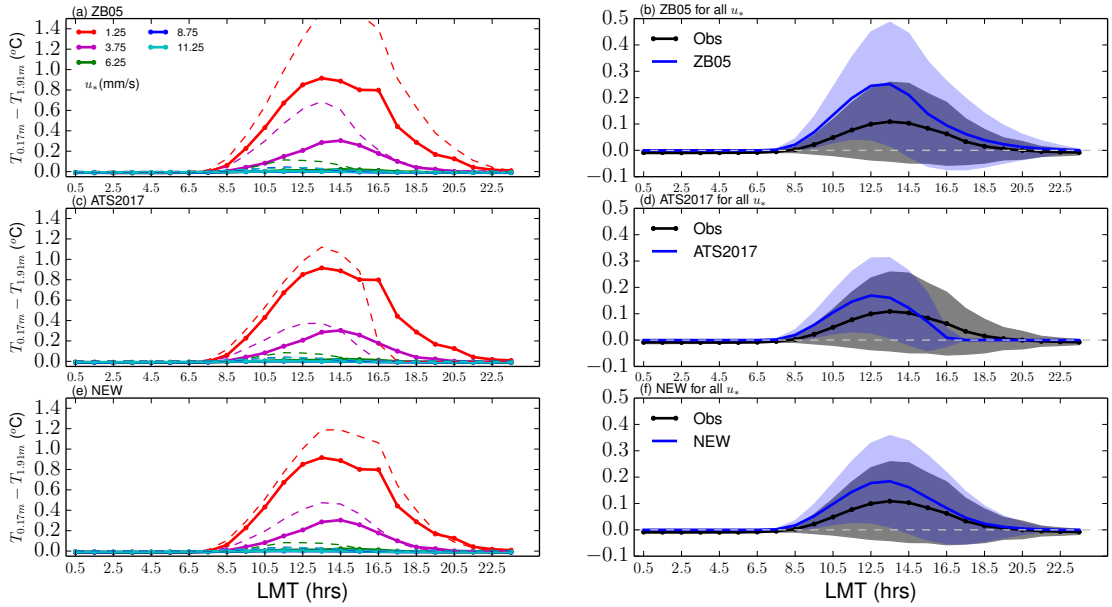

Figure 16: Same as Fig. 15 but for the Arabian Sea.

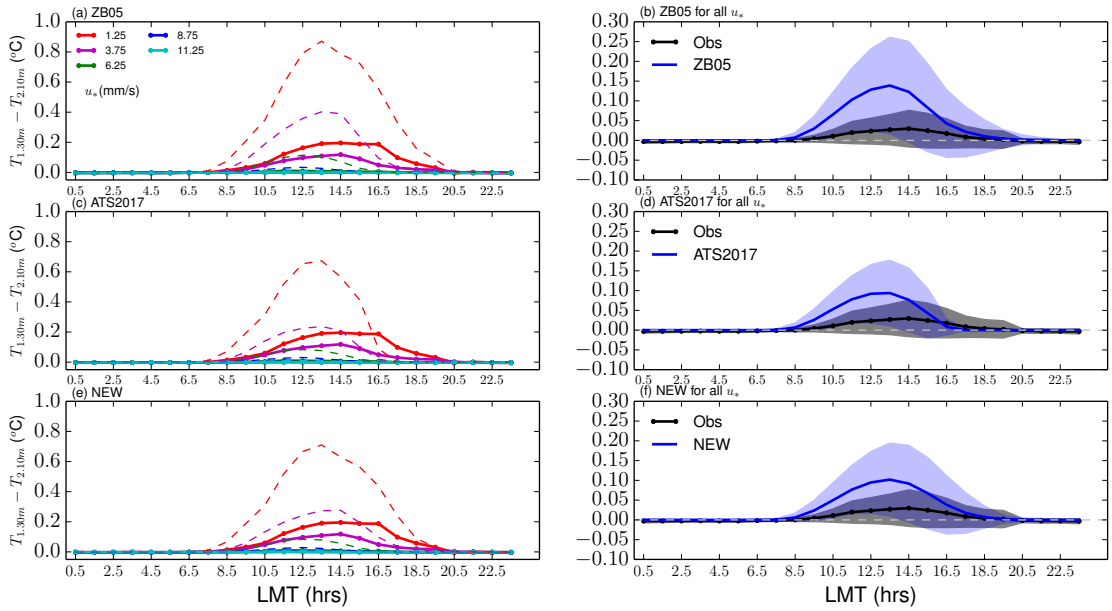

Figure 17: Same as Fig. 15 but for the Spurs-1.

5 Summary and conclusions

It is imperative for the GMAO to develop an IESA that includes an Atmosphere-Ocean CDAS. To achieve this goal, the GEOS GCM needs to be flexible enough to support the GMAO "Forward Processing" (FP) system which implements an ADAS that in-turn relies on an AGCM, and also the future AO-CDAS that would use the AOGCM. The AOIL has been formulated as a computationally effective approach to support both the AGCM and AOGCM. It also simulates the near-surface variations over the ocean, for satellite radiance data assimilation at negligible expense. This AOIL can be embedded into the top layer of the OGCM if the GEOS GCM is exercised in coupled, AOGCM mode. In uncoupled (AGCM) mode, with minor modifications, it provides the same functionality by reading in the required oceanic fields from existing data sets. The present formulation of the AOIL provides means to simulate near-surface diurnal warming and cool-skin effects; treatment of other variables such as surface salinity and sea-ice is left for future work. We also formulated and tested improvements to the diurnal warming model formulation that is currently being used in the GMAO ADAS. Offline model tests with buoy measurements demonstrate that the proposed formulation does not have the sharp drop in diurnal warming seen in the current operational version.

The next step is to implement this formulation of the AOIL into the GEOS GCM and establish an improved diurnal warming cycle in the GEOS ADAS and FP system. Thereafter we will proceed with the AO-CDAS development. As we learn from time-series of near-surface ocean observations and departures of model predictions from these observations, we anticipate further refinements to this formulation- perhaps an increase in its vertical resolution or a revamping of the formulation into more comprehensive mixed layer model. To a large extent the version and resolution of the OGCM will be key factors in these developments.

6 Acknowledgments

We thank the Woods Hole Oceanographic Institution for making the data used in this study publicly available. Computations were carried out on the Discover cluster of NASA- NCCS at the Goddard Space Flight Center.

References

Akella S, Todling R, Suarez M. 2016. Estimation of the ocean skin temperature using the NASA GEOS Atmospheric Data Assimilation System. Technical Report Series on Global Modeling and Data Assimilation NASA/TM-2016-104606/Vol 44, NASA Goddard Space Flight Center, URL https://gmao.gsfc.nasa.gov/pubs/docs/Akella873.pdf.

Akella S, Todling R, Suarez M. 2017. Assimilation for skin SST in the NASA GEOS atmospheric data assimilation system. *Quarterly Journal of the Royal Meteorological Society* **143**(703): 1032–1046, doi:10.1002/qj.2988.

Alderson SG. 1990. On embedding a mixed layer model into an ocean general circulation model. *Dynamics of Atmospheres and Oceans* **15**(1-2): 59–86.

Bentsen M, Bethke I, Debernard JB, Iversen T, Kirkevåg A, Seland Ø, Drange H, Roelandt C, Seierstad IA, Hoose C, Kristjánsson JE. 2013. The norwegian earth system model, noresm1-m ââĆň" part 1: Description and basic evaluation of the physical climate. *Geoscientific Model Development* **6**(3): 687–720, doi:10.5194/gmd-6-687-2013, URL https://www.geosci-model-dev.net/6/687/2013/.

Borovikov A, Cullather R, Kovach R, Marshak J, Vernieres G, Vikhliaev Y, Zhao B, Li Z. 2017. GEOS-5 seasonal forecast system. *Climate Dynamics* doi:10.1007/s00382-017-3835-2.

Boutin J, Chao Y, Asher WE, Delcroix T, Drucker R, Drushka K, Kolodziejczyk N, Lee T, Reul N, Reverdin G, Schanze J, Soloviev A, Yu L, Anderson J, Brucker L, Dinnat E, Santos-Garcia A, Jones WL, Maes C, Meissner T, Tang W, Vinogradova N, Ward B. 2016. Satellite and in situ salinity: Understanding near-surface stratification and subfootprint variability. *Bulletin of the American Meteorological Society* **97**(8): 1391–1407, doi:10.1175/BAMS-D-15-00032.1.

Brassington GB, Martin MJ, Tolman HL, Akella S, Balmeseda M, Chambers CRS, Chassignet E, Cummings JA, Drillet Y, Jansen PAEM, Laloyaux P, Lea D, Mehra A, Mirouze I, Ritchie H, Samson G, Sandery PA, Smith GC, Suarez M, Todling R. 2015. Progress and challenges in short- to medium-range coupled prediction. *J Operational Oceanography.* **8**: s239– s258, doi:10.1080/1755876X.2015.1049875.

Curry JA, Bentamy A, Bourassa MA, Bourras D, Bradley EF, Brunke M, Castro S, Chou SH, Clayson CA, Emery WJ, Eymard L, Fairall CW, Kubota M, Lin B, Perrie W, Reeder RA, Renfrew IA, Rossow WB, Rossow WB, Schulz J, Smith SR, Webster PJ, Wick GA, Zeng X. 2004. Seaflux. *Bull. Amer. Meteor. Soc.* **85**: 409–424, doi:http://dx.doi.org/10.1175/BAMS-85-3-409.

Dee DP, Balmaseda M, Balsamo G, Engelen R, Simmons AJ, Thépaut JN. 2014. Toward a consistent reanalysis of the climate system. *Bull. Amer. Meteor. Soc.* **95**: 1235–1248, doi:http://dx.doi.org/10.1175/BAMS-D-13-00043.1.

Delworth TL, Broccoli AJ, Rosati A, Stouffer RJ, Balaji V, Beesley JA, Cooke WF, Dixon KW, Dunne J, Dunne KA, Durachta JW, Findell KL, Ginoux P, Gnanadesikan A, Gordon CT, Griffies SM, Gudgel R, Harrison MJ, Held IM, Hemler RS, Horowitz LW, Klein SA, Knutson TR, Kushner PJ, Langenhorst AR, Lee HC, Lin SJ, Lu J, Malyshev SL, Milly PCD, Ramaswamy V, Russell J, Schwarzkopf MD, Shevliakova E, Sirutis JJ, Spelman MJ, Stern WF, Winton M, Wittenberg AT, Wyman B, Zeng F, Zhang R. 2006. GFDL's CM2 Global Coupled Climate Models. Part i: Formulation and simulation characteristics. *Journal of Climate* **19**(5): 643–674, doi:10.1175/JCLI3629.1.

Fairall CW, Bradley EF, Godfrey JS, Wick GA, Edson JB, Young GS. 1996. Cool-skin and warm-layer effects on sea surface temperature. *J Geophys Res-Oceans* **101**: 1295–1308, doi:10.1029/95JC03190.

Gelaro R, McCarty W, Suárez MJ, Todling R, Molod A, Takacs L, Randles CA, Darmenov A, Bosilovich MG, Reichle R, Wargan K, Coy L, Cullather R, Draper C, Akella S, Buchard V, Conaty A, da Silva AM, Gu W, Kim GK, Koster R, Lucchesi R, Merkova D, Nielsen JE, Partyka G, Pawson S, Putman W, Rienecker M, Schubert SD, Sienkiewicz M, Zhao B. 2017. The modern-era retrospective analysis for research and applications, version 2 (MERRA-2). *Journal of Climate* **30**(14): 5419–5454, doi:10.1175/JCLI-D-16-0758.1.

Gentemann CL, Akella S. 2018. Evaluation of NASA GEOS-ADAS modeled diurnal warming through comparisons to SEVIRI and AMSR2 SST observations. *Journal of Geophysical Research: Oceans* **123**(2): 1364–1375, doi:10.1002/2017JC013186.

Ham YG, Rienecker MM, Suarez MJ, Vikhliaev Y, Zhao B, Marshak J, Vernieres G, Schubert SD. 2014. Decadal prediction skill in the GEOS-5 forecast system. *Clim Dyn* **42**: 1–20, doi:10.1007/s00382-013-1858-x.

Hewitt HT, Copsey D, Culverwell ID, Harris CM, Hill RSR, Keen AB, McLaren AJ, Hunke EC. 2011. Design and implementation of the infrastructure of hadgem3: the next-generation met office climate modelling system. *Geoscientific Model Development* **4**(2): 223–253, doi:10.5194/gmd-4-223-2011, URL https://www.geosci-model-dev.net/4/223/2011/.

Horrocks LA, Candy B, Nightingale TJ, Saunders RW, O'Carroll A, Harris AR. 2003. Parameterizations of the ocean skin effect and implications for satellite-based measurement of sea-surface temperature. *Journal of Geophysical Research: Oceans* **108**(C3).

Large WG, Caron JM. 2015. Diurnal cycling of sea surface temperature, salinity, and current in the CESM coupled climate model. *Journal of Geophysical Research: Oceans* **120**(5): 3711–3729, doi:10.1002/2014JC010691, URL http://dx.doi.org/10.1002/2014JC010691.

Li X, Sui CH, Lau KM, Adamec D. 2000. Effects of precipitation on ocean mixed-layer temperature and salinity as simulated in a 2-d coupled ocean-cloud resolving atmosphere model. *Journal of the Meteorological Society of Japan. Ser. II* **78**(5): 647–659, doi:10.2151/jmsj1965.78.5_647.

Mogensen K, Keeley S, Towers P. 2012. *Coupling of the nemo and ifs models in a single executable*. European Centre for Medium-Range Weather Forecasts.

Molod A, Takacs L, Suarez M, Bacmeister J. 2015. Development of the GEOS-5 atmospheric general circulation model: evolution from MERRA to MERRA2. *Geoscientific Model Development* **8**(5): 1339–1356, doi:10.5194/gmd-8-1339-2015.

Molod A, Takacs L, Suarez M, Bacmeister J, Song IS, Eichmann A. 2012. The GEOS-5 Atmospheric General Circulation Model: Mean Climate and Development from MERRA to Fortuna. Technical Report Series on Global Modeling and Data Assimilation NASA/TM-2012-104606/Vol 28, NASA Goddard Space Flight Center.

National Academies of Sciences, Engineering, and Medicine. 2018. *Thriving on our changing planet: A decadal strategy for earth observation from space*. The National Academies Press: Washington, DC, ISBN 978-0-309-46754-4, doi:10.17226/24938, URL https://www.nap.edu/catalog/24938/thriving-on-our-changing-planet-a-decadal-strategy-for-earth.

National Research Council. 1992. *Oceanography in the next decade: Building new partnerships*. The National Academies Press: Washington, DC, ISBN 978-0-309-04794-4, doi:10.17226/2048, URL https://www.nap.edu/catalog/2048/oceanography-in-the-next-decade-building-new-partnerships.

Navon I. 1998. Practical and theoretical aspects of adjoint parameter estimation and identifiability in meteorology and oceanography. *Dynamics of Atmospheres and Oceans* **27**(1): 55 – 79, doi:https://doi.org/10.1016/S0377-0265(97)00032-8, URL http://www.sciencedirect.com/science/article/pii/S0377026597000328.

Saunders PM. 1967. The Temperature at the Ocean-Air Interface. *J Atmos Sci* **24**: 269–273.

Schiller A, Godfrey J. 2005. A diagnostic model of the diurnal cycle of sea surface temperature for use in coupled ocean-atmosphere models. *Journal of Geophysical Research: Oceans* **110**(C11).

Schneider N, Müller P. 1990. The meridional and seasonal structures of the mixed-layer depth and its diurnal amplitude observed during the Hawaii-to-Tahiti Shuttle Experiment. *Journal of Physical Oceanography* **20**(9): 1395–1404, doi:10.1175/1520-0485(1990)020<1395:TMASSO>2.0.CO;2.

Shinoda T, Hendon HH. 1998. Mixed layer modeling of intraseasonal variability in the tropical western Pacific and Indian oceans. *Journal of Climate* **11**(10): 2668–2685, doi:10.1175/1520-0442(1998)011<2668:MLMOIV>2.0.CO;2.

Soloviev AV. 1982. On the vertical structure of the ocean thin surface layer at light wind. *Dokl. Acad. Sci. USSR Earth Sci. Sect. Engl. Transl.* **18**: 751–760.

Takaya Y, Bidlot JR, Beljaars ACM, Janssen PAEM. 2010. Refinements to a prognostic scheme of skin sea surface temperature. *J Geophys Res-Oceans* **115**: C06 009, doi:10.1029/2009JC005985.

Todling R, El Akkraoui A. 2018. The GMAO Hybrid Ensemble-Variational Atmospheric Data Assimilation System: Version 2.0. Technical Report Series on Global Modeling and Data Assimilation NASA/TM-2018-104606/Vol 50, NASA Goddard Space Flight Center, URL https://gmao.gsfc.nasa.gov/pubs/docs/Todling1019.pdf.

Turner JS. 1979. *Buoyancy effects in fluids*. Cambridge University Press.

Vernieres G, Rienecker MM, Kovach R, Keppenne CL. 2012. The GEOS-iODAS: Description and Evaluation. Technical Report Series on Global Modeling and Data Assimilation NASA/TM-2012-104606/Vol 30, NASA Goddard Space Flight Center.

Weller R, Anderson S. 1996. Surface meteorology and air-sea fluxes in the western equatorial pacific warm pool during the toga coupled ocean-atmosphere response experiment. *Journal of Climate* **9**(8): 1959–1990, doi:https://doi.org/10.1175/1520-0442(1996)009<1959:SMAASF>2.0.CO;2.

While J, Mao C, Martin M, Roberts-Jones J, Sykes P, Good S, McLaren A. 2017. An operational analysis system for the global diurnal cycle of sea surface temperature: implementation and validation. *Quarterly Journal of the Royal Meteorological Society* **143**(705): 1787–1803, doi:10.1002/qj.3036.

While J, Martin M. 2013. Development of a variational data assimilation system for the diurnal cycle of sea surface temperature. *J Geophys Res-Oceans* **118**: 2845–2862, doi:doi:10.1002/jgrc.20215.

Zeng X, Ackerman S, Ferraro RD, Lee TJ, Murray JJ, Pawson S, Reynolds C, Teixeira J. 2016. Challenges and opportunities in NASA weather research. *Bulletin of the American Meteorological Society* **97**(7): ES137–ES140, doi:10.1175/BAMS-D-15-00195.1.

Zeng X, Beljaars A. 2005. A prognostic scheme of sea surface skin temperature for modeling and data assimilation. *Geophys Res Lett* **32**(14): L14 605, doi:10.1029/2005GL023030.

Appendix A. Acronyms

ADAS atmospheric data assimilation system

AGCM atmospheric general circulation model

AOGCM atmosphere ocean general circulation model

AOIL atmosphere-ocean interface layer

DAS data assimilation system

CDAS coupled data assimilation system

ECMWF European Center for Medium-Range Weather Forecasts

GCM general circulation model

GEOS Goddard Earth Observing System

GFDL Geophysical Fluid Dynamics Laboratory

GMAO Global Modeling and Assimilation Office

IESA integrated earth system analysis

MERRA Modern-Era Retrospective Analysis For Research and Applications

NASA National Aeronautics and Space Administration

OGCM ocean general circulation model

SST sea surface temperature

WWRP World Weather Research Program

Appendix B. Cool skin layer

Here we briefly describe the calculations in the cool-skin layer. This layer lies just below the air-sea interface and has a thickness of a few millimeters. It is cooled by longwave, sensible, and latent heat fluxes to the atmosphere. See Curry *et al.* (2004); Saunders (1967); see also Horrocks *et al.* (2003) and references therein for more details on the importance of its inclusion from a satellite radiance perspective. But because it is so thin, it cannot be warmed by solar fluxes below the surface; the heat leaving the ocean's surface can only be balanced by molecular diffusion. We follow Fairall *et al.* (1996) and ZB05 in assuming the diffusive flux is constant within this layer, leading to a temperature drop,

$$\Delta T_c = T_\delta - T_s = \max\left(\frac{\delta}{\rho_w\, c_w\, k_w} Q^c_{net}, 0\right), \tag{B.1}$$

where ρ_w, c_w, and k_w denote density, heat capacity and thermal conductivity of sea water, respectively. The layer thickness δ is assumed to be proportional to the Kolmogorov scale, $\frac{\nu_w}{\varepsilon}$, where ν_w is the kinematic viscosity of seawater and $\varepsilon \propto \frac{u_*}{\delta}$ is the turbulent dissipation rate, with

$$\delta = \frac{\lambda\, \nu_w}{u_*}. \tag{B.2}$$

The friction velocity over water is given by $u_* = u_{*,a}\sqrt{\rho_a/\rho_w}$, $u_{*,a}$ is the atmosphere friction velocity and ρ_a is air density. Q^c_{net} is the net heat flux in the cool layer, which depends on the non-solar fluxes $Q^\downarrow$ in Eq. (9) and only a fraction of the net downward surface shortwave flux (SW_{top}):

$$Q^c_{net} = Q^\downarrow - f_c\, SW_{top}. \tag{B.3}$$

Following ATS17 and ZB05, $f_c = 0.065 + 11\,\delta - \frac{6.6\times10^{-5}}{\delta}\left[1 - \exp\left(-\frac{\delta}{8\times10^{-4}}\right)\right]$. The Saunders parameter, λ, is computed as in Fairall *et al.* (1996):

$$\lambda = 6\left[1 + \left\{\left(\frac{\alpha_w\, g\, F^v_B}{\rho_w\, c_w}\right)\left(\frac{16\,\rho_w^2\, c_w^2\, \nu_w^3}{\kappa_w^2}\right)\frac{1}{u^4_{*,w}}\right\}^{3/4}\right]^{-1/3}, \tag{B.4}$$

where g denotes the acceleration due to gravity and α_w is the water thermal expansion coefficient. Here, F^v_B is the virtual surface buoyancy flux:

$$F^v_B = Q^\downarrow + \left(\frac{S\beta c_w}{\alpha_w L_e}\right) H_l, \tag{B.5}$$

where L_e denotes the latent heat of vaporization of seawater, S is the mean salinity, and β is its expansion coefficient. We follow Fairall *et al.* (1996) to set $S\beta = 0.026$. However, as shown by Saunders (1967), Turner (1979) and Boutin *et al.* (2016) and references therein, the near-surface salinity varies with the evaporation rate. Future refinement and revision of the AOIL, will include some of these effects in the calculation of F^v_B.

Appendix C. Recommendations for seasonal forecasting applications

The following remarks and suggestions are for the developers and potential users of the seasonal forecasting system.

- As already stated and formulated in Eq. (11), the formulation of the present AOIL does not imply any change to the OGCM.
- If the AOIL is absent, then the OGCM top layer temperature, T_o, is equal to the AGCM skin SST, T_s. By the same token, in the presence of the AOIL, the OGCM is impacted by it only via indirect feedbacks through the non-solar fluxes, $Q^{\downarrow}$. These fluxes depend on T_s as calculated by the AOIL with the inclusion of near-surface variability.
- If the OGCM has more than one vertical level in the top 10m (i.e., the top level thickness, D, is less than < 10m), then one simple possibility (as used at the ECMWF; Kristian Mogensen, personal communication, 2018) is to simply set $T_s = T_o - \Delta T_c$. (The thickness of the top level in the ECMWF OGCM is 2m.)
- The present formulation of the AOIL is for near-surface temperature variations only, and the main driver for its development is satellite radiance data assimilation[C1]. For other oceanic variables such as the OGCM-calculated salinity and sea-ice (thickness, temperature, etc), we recommend that these variables be used by the AGCM without any change. For example, the OGCM top level salinity, S_o, would be equal to the sea surface salinity, and to solve for S_o, the OGCM would be given the rates of evaporation, precipitation, run-off and snow melt from the AGCM (similar to Hewitt *et al.* (2011)).

[C1] This does not apply to the seasonal forecasting systems since they do not analyze their atmospheric state (Borovikov *et al.*, 2017).

Previous Volumes in This Series

Volume 1 *September 1994*
Documentation of the Goddard Earth Observing System (GEOS) general circulation model - Version 1
L. L. Takacs, A. Molod, and T. Wang

Volume 2 *October 1994*
Direct solution of the implicit formulation of fourth order horizontal diffusion for gridpoint models on the sphere
Y. Li, S. Moorthi, and J. R. Bates

Volume 3 *December 1994*
An efficient thermal infrared radiation parameterization for use in general circulation models
M.-D. Chou and M. J. Suarez

Volume 4 *January 1995*
Documentation of the Goddard Earth Observing System (GEOS) Data Assimilation System - Version 1
James Pfaendtner, Stephen Bloom, David Lamich, Michael Seablom, Meta Sienkiewicz, James Stobie, and Arlindo da Silva

Volume 5 *April 1995*
Documentation of the Aries-GEOS dynamical core: Version 2
Max J. Suarez and Lawrence L. Takacs

Volume 6 *April 1995*
A Multiyear Assimilation with the GEOS-1 System: Overview and Results
Siegfried Schubert, Chung-Kyu Park, Chung-Yu Wu, Wayne Higgins, Yelena Kondratyeva, Andrea Molod, Lawrence Takacs, Michael Seablom, and Richard Rood

Volume 7 *September 1995*
Proceedings of the Workshop on the GEOS-1 Five-Year Assimilation
Siegfried D. Schubert and Richard B. Rood

Volume 8 *March 1996*
Documentation of the Tangent Linear Model and Its Adjoint of the Adiabatic Version of the NASA GEOS-1 C-Grid GCM: Version 5.2
Weiyu Yang and I. Michael Navon

Volume 9 *March 1996*
Energy and Water Balance Calculations in the Mosaic LSM
Randal D. Koster and Max J. Suarez

Volume 10 *April 1996*
Dynamical Aspects of Climate Simulations Using the GEOS General Circulation Model
Lawrence L. Takacs and Max J. Suarez

Volume 11 *May 1997*
Documentation of the Tangent Linear and its Adjoint Models of the Relaxed Arakawa-Schubert Moisture Parameterization Package of the NASA GEOS-1 GCM (Version 5.2)
Weiyu Yang, I. Michael Navon, and Ricardo Todling

Volume 12 *August 1997*
Comparison of Satellite Global Rainfall Algorithms
Alfred T. C. Chang and Long S. Chiu

Volume 13 *December 1997*
Interannual Variability and Potential Predictability in Reanalysis Products
Wie Ming and Siegfried D. Schubert

Volume 14 *August 1998*
A Comparison of GEOS Assimilated Data with FIFE Observations
Michael G. Bosilovich and Siegfried D. Schubert

Volume 15 *June 1999*
A Solar Radiation Parameterization for Atmospheric Studies
Ming-Dah Chou and Max J. Suarez

Volume 16 *November 1999*
Filtering Techniques on a Stretched Grid General Circulation Model
Lawrence Takacs, William Sawyer, Max J. Suarez, and Michael S. Fox-Rabinowitz

Volume 17 *July 2000*
Atlas of Seasonal Means Simulated by the NSIPP-1 Atmospheric GCM
Julio T. Bacmeister, Philip J. Pegion, Siegfried D. Schubert, and Max J. Suarez

Volume 18 *December 2000*
An Assessment of the Predictability of Northern Winter Seasonal Means with the NSIPP1 AGCM
Philip J. Pegion, Siegfried D. Schubert, and Max J. Suarez

Volume 19 *July 2001*
A Thermal Infrared Radiation Parameterization for Atmospheric Studies
Ming-Dah Chou, Max J. Suarez, Xin-Zhong, and Michael M.-H. Yan

Volume 20 *August 2001*
The Climate of the FVCCM-3 Model
Yehui Chang, Siegfried D. Schubert, Shian-Jiann Lin, Sharon Nebuda, and Bo-Wen Shen

Volume 21 *September 2001*
Design and Implementation of a Parallel Multivariate Ensemble Kalman Filter for the Poseidon Ocean General Circulation Model
Christian L. Keppenne and Michele M. Rienecker

Volume 22 *August 2002*
Coupled Ocean-Atmosphere Radiative Model for Global Ocean Biogeochemical Models
Watson W. Gregg

Volume 23 *November 2002*
Prospects for Improved Forecasts of Weather and Short-term Climate Variability on Subseasonal (2-Week to 2-Month) Time Scales
Siegfried D. Schubert, Randall Dole, Huang van den Dool, Max J. Suarez, and Duane Waliser

Volume 24 *July 2003*
Temperature Data Assimilation with Salinity Corrections: Validation for the NSIPP Ocean Data Assimilation System in the Tropical Pacific Ocean, 1993–1998
Alberto Troccoli, Michele M. Rienecker, Christian L. Keppenne, and Gregory C. Johnson

Volume 25 *December 2003*
Modeling, Simulation, and Forecasting of Subseasonal Variability
Duane Waliser, Siegfried D. Schubert, Arun Kumar, Klaus Weickmann, and Randall Dole

Volume 26 *April 2005*
Documentation and Validation of the Goddard Earth Observing System (GEOS) Data Assimilation System - Version 4
Senior Authors: S. Bloom, A. da Silva and D. Dee
Contributing Authors: M. Bosilovich, J-D. Chern, S. Pawson, S. Schubert, M. Sienkiewicz, I. Stajner, W-W. Tan, and M-L. Wu

Volume 27 *December 2008*
The GEOS-5 Data Assimilation System - Documentation of Versions 5.0.1, 5.1.0, and 5.2.0
M. M. Rienecker, M. J. Suarez, R. Todling, J. Bacmeister, L. Takacs, H.-C. Liu, W. Gu, M. Sienkiewicz, R. D. Koster, R. Gelaro, I. Stajner, and J. E. Nielsen

Volume 28 *April 2012*
The GEOS-5 Atmospheric General Circulation Model: Mean Climate and Development from MERRA to Fortuna
Andrea Molod, Lawrence Takacs, Max Suarez, Julio Bacmeister, In-Sun Song, and Andrew Eichmann

Volume 29 *May 2012*
Atmospheric Reanalyses âĂŞ Recent Progress and Prospects for the Future. A Report from a Technical Workshop, April 2010
Michele M. Rienecker, Dick Dee, Jack Woollen, Gilbert P. Compo, Kazutoshi Onogi, Ron Gelaro, Michael G. Bosilovich, Arlindo da Silva, Steven Pawson, Siegfried Schubert, Max Suarez, Dale Barker, Hirotaka Kamahori, Robert Kistler, and Suranjana Saha

Volume 30 *September 2012*
The GEOS-ODAS, Description and Evaluation
Guillaume Vernieres, Michele M. Rienecker, Robin Kovach and Christian L. Keppenne

Volume 31 *March 2013*
Global Surface Ocean Carbon Estimates in a Model Forced by MERRA
Watson W. Gregg, Nancy W. Casey, and Cécile S. Rousseaux

Volume 32 *March 2014*
Estimates of AOD Trends (2002–2012) over the World's Major Cities based on the MERRA Aerosol Reanalysis
Simon Provençal, Pavel Kishcha, Emily Elhacham, Arlindo M. da Silva and Pinhas Alpert

Volume 33 *August 2014*
The Effects of Chlorophyll Assimilation on Carbon Fluxes in a Global Biogeochemical Model
Cécile S. Rousseaux and Watson W. Gregg

Volume 34 *September 2014*
Background Error Covariance Estimation using Information from a Single Model Trajectory with Application to Ocean Data Assimilation into the GEOS-5 Coupled Model
Christian L. Keppenne, Michele M. Rienecker, Robin M. Kovach, and Guillaume Vernieres

Volume 35 *December 2014*
Observation-Corrected Precipitation Estimates in GEOS-5
Rolf H. Reichle and Qing Liu

Volume 36 *March 2015*
Evaluation of the 7-km GEOS-5 Nature Run
Ronald Gelaro, William M. Putman, Steven Pawson, Clara Draper, Andrea Molod, Peter M. Norris, Lesley Ott, Nikki Privé, Oreste Reale, Deepthi Achuthavarier, Michael Bosilovich, Virginie Buchard, Winston Chao, Lawrence Coy, Richard Cullather, Arlindo da Silva, Anton Darmenov, Ronald M. Errico, Marangelly Fuentes, Min-Jeong Kim, Randal Koster, Will McCarty, Jyothi Nattala, Gary Partyka, Siegfried Schubert, Guillaume Vernieres, Yuri Vikhliaev, and Krzysztof Wargan

Volume 37 *March 2015*
Maintaining Atmospheric Mass and Water Balance Within Reanalysis
Lawrence L. Takacs, Max Suarez, and Ricardo Todling

Volume 38 *September 2015*
The Quick Fire Emissions Dataset (QFED): Documentation of versions 2.1, 2.2 and 2.4
Anton Darmenov and Arlindo da Silva

Volume 39 *September 2015*
Land Boundary Conditions for the Goddard Earth Observing System Model Version 5 (GEOS-5) Climate Modeling System - Recent Updates and Data File Descriptions
Sarith Mahanama, Randal Koster, Gregory Walker, Lawrence Takacs, Rolf Reichle, Gabrielle De Lannoy, Qing Liu, Bin Zhao, and Max Suarez

Volume 40 *October 2015*
Soil Moisture Active Passive (SMAP) Project Assessment Report for the Beta-Release L4_SM Data Product
Rolf H. Reichle, Gabrielle J. M. De Lannoy, Qing Liu, Andreas Colliander, Austin Conaty, Thomas Jackson, John Kimball, and Randal D. Koster

Volume 41 *October 2015*
GDIS Workshop Report
Schubert, Siegfried, Will Pozzi, Kingtse Mo, Eric Wood, Kerstin Stahl, Mike Hayes, Juergen Vogt, Sonia Seneviratne, Ron Stewart, Roger Pulwarty, and Robert Stefanski

Volume 42 *November 2015*
Soil Moisture Active Passive (SMAP) Project Calibration and Validation for the L4_C Beta-Release Data Product
John Kimball, Lucas Jones, Joseph Glassy, E. Natasha Stavros, Nima Madani, Rolf Reichle, Thomas Jackson, and Andreas Colliander

Volume 43 *September 2015*
MERRA-2: Initial Evaluation of the Climate
Michael G. Bosilovich, Santha Akella, Lawrence Coy, Richard Cullather, Clara Draper, Ronald Gelaro, Robin Kovach, Qing Liu, Andrea Molod, Peter Norris, Krzysztof Wargan, Winston Chao, Rolf Reichle, Lawrence Takacs, Yury Vikhliaev, Steve Bloom, Allison Collow, Stacey Firth, Gordon Labow, Gary Partyka, Steven Pawson, Oreste Reale, Siegfried D. Schubert, and Max Suarez

Volume 44 *February 2016*
Estimation of the Ocean Skin Temperature using the NASA GEOS Atmospheric Data Assimilation System
Santha Akella, Ricardo Todling and Max Suarez

Volume 45
December 2016

The MERRA-2 Aerosol Assimilation. NASA Technical Report Series on Global Modeling and Data Assimilation

C. A. Randles, A. M. da Silva, V. Buchard, A. Darmenov, P. R. Colarco, V. Aquila, H. Bian, E. P. Nowottnick, X. Pan, A. Smirnov, H. Yu, and R. Govindaraju

Volume 46
October 2016

MERRA-2 Input Observations: Summary and Assessment

Will McCarty, Lawrence Coy, Ronald Gelaro, Albert Huang, Dagmar Merkova, Edmond B. Smith, Meta Seinkiewicz, and Krzysztof Wargan

Volume 47
May 2017

An Evaluation of Teleconnections Over the United States in an Ensemble of AMIP Simulations with the MERRA-2 Configuration of the GEOS Atmospheric Model.

Allison B. Marquardt Collow, Sarith P. Mahanama, Michael G. Bosilovich, Randal D. Koster, and Siegfried D. Schubert

Volume 48
July 2017

Description of the GMAO OSSE for Weather Analysis Software Package: Version 3

Ronald M Errico, Nikki C. Privé, David Carvalho, Meta Sienkiewicz, Amal El Akkraoui, Jing Guo, Ricardo Todling, Will McCarty, William M. Putman, Arlindo da Silva, Ronald Gelaro, Isaac Moradi

Volume 49
March 2018

Preliminary evaluation of influence of aerosols on the simulation of brightness temperature in the NASA Goddard Earth Observing System Atmospheric Data Assimilation System

Jong Kim, Santha Akella, Will McCarty, Ricardo Todling and Arlindo M. da Silva

Volume 50
March 2018

The GMAO Hybrid Ensemble-Variational Atmospheric Data Assimilation System: Version 2.0

Ricardo Todling and Amal El Akkraoui